

Remote Sensing Supplemental Materials for
Climate Sensitivity of High Arctic Permafrost Terrain Demonstrated by Widespread Ice-Wedge Thermokarst on Banks Island

Robert H. Fraser, Steven V. Kokelj, Trevor C. Lantz, Morgan McFarlane-Winchester, Ian Olthof, and Denis Lacelle

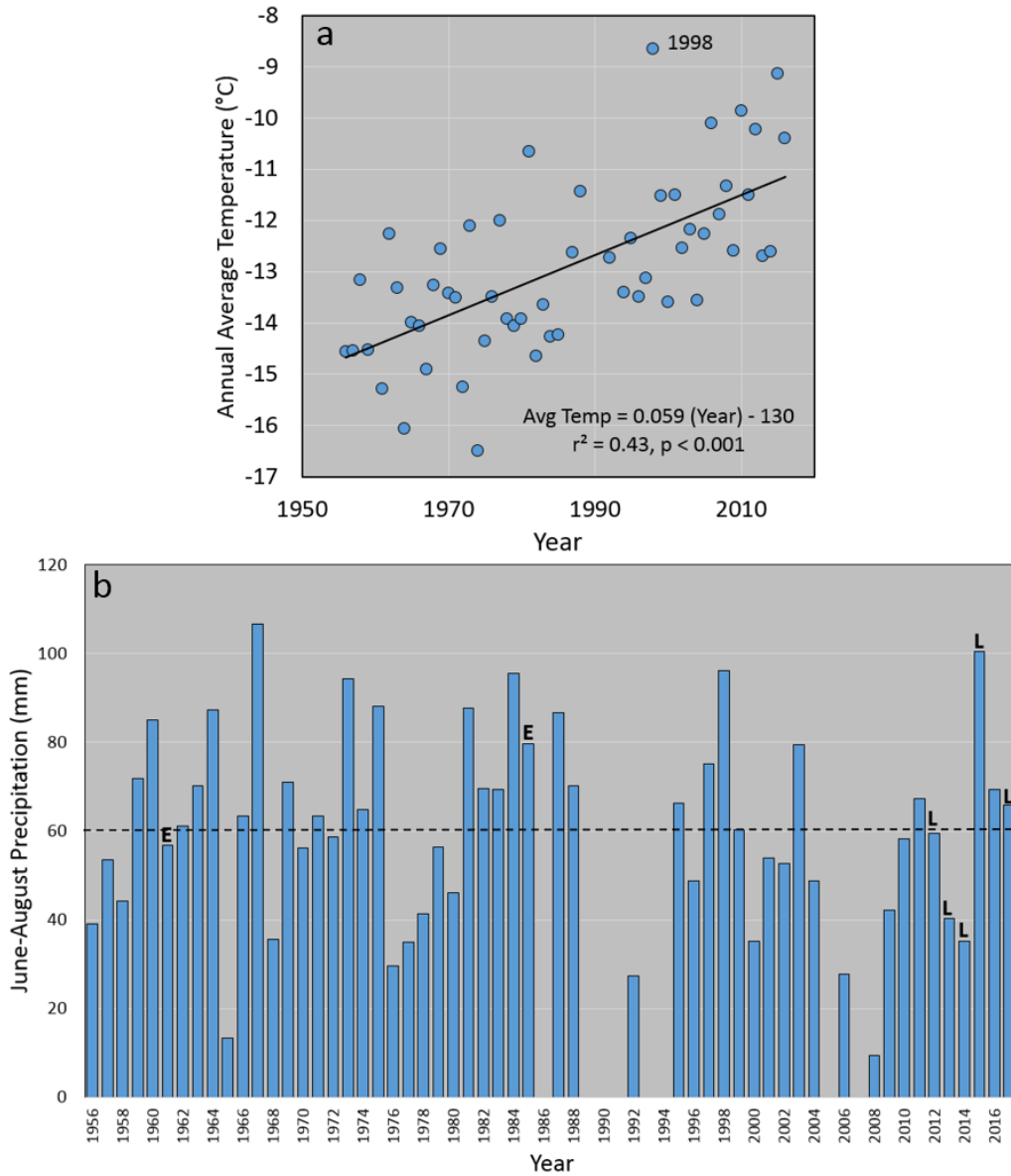


Figure S1. (a) Annual average temperature (1959-2016) summarized using Environment Canada weather station data from Sachs Harbour, Banks Island with best-fit linear regression line ($p < 0.05$) shown. The long-term mean for annual average temperature is $-12.9\text{ }^{\circ}\text{C}$; (b) Annual June-August summer precipitation measured at Sachs Harbour shows no long-term trend and no single-year extreme values that would potentially bias wetness in the early, baseline images (E) or late, melt pond images (L), with the exception of one WorldView image from 2015. Long-term mean June-August precipitation indicated with a dashed line is 60 mm .



Figure S2. Thin till veneer over relict massive ice and wedge ice (Table S2, Site 1). Arrow in foreground indicates the trough of a large ice-wedge about 3 m width. Arrow in background indicates thin veneer of soils overlying massive ice. Drilling on August 1, 2015 indicated that active layer thaw had truncated wedge ice.



Figure S3. Thaw slump headwall in Aulavik National Park, Banks Island showing large flat-topped ice wedges truncated by a thin active layer. Photo from August 2017 provided courtesy of Aurora Research Institute and Parks Canada Agency.



Figure S4. Thaw slump headwall in Aulavik National Park, Banks Island showing thaw slump in high centred polygonal terrain. Ice wedges are exposed and truncated by the developing active layer. Downslope runoff along ice-wedge trough has accelerated back wasting of headwall on left side. Photo from August 2017 provided courtesy of Aurora Research Institute and Parks Canada Agency.

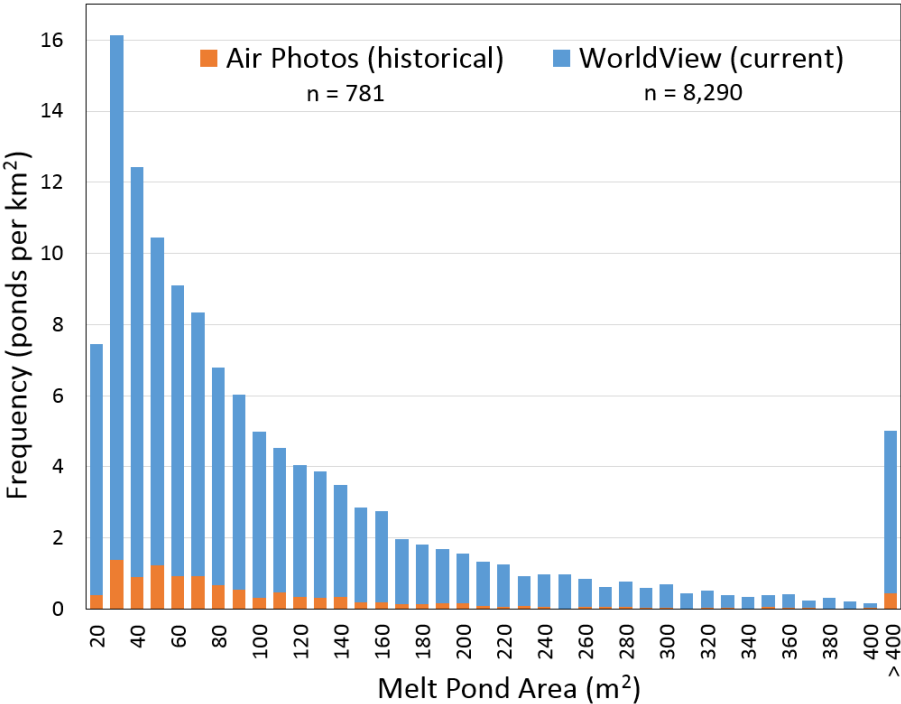
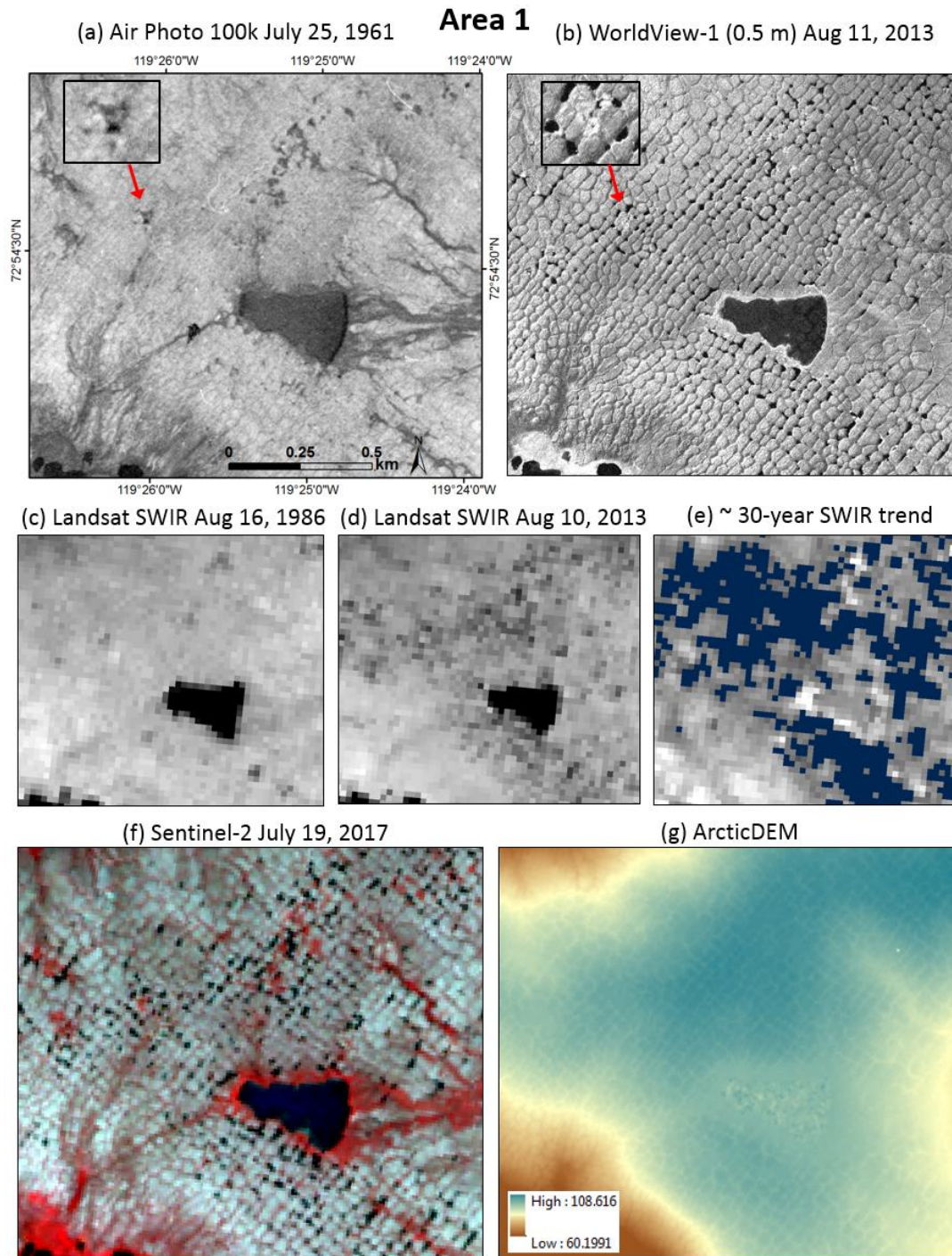


Figure S5. Stacked column chart showing the frequency distribution of upland ice-wedge melt pond areas extracted for the eight high resolution study areas using air photos (1958-1961) and WorldView satellite imagery (2013-2017).

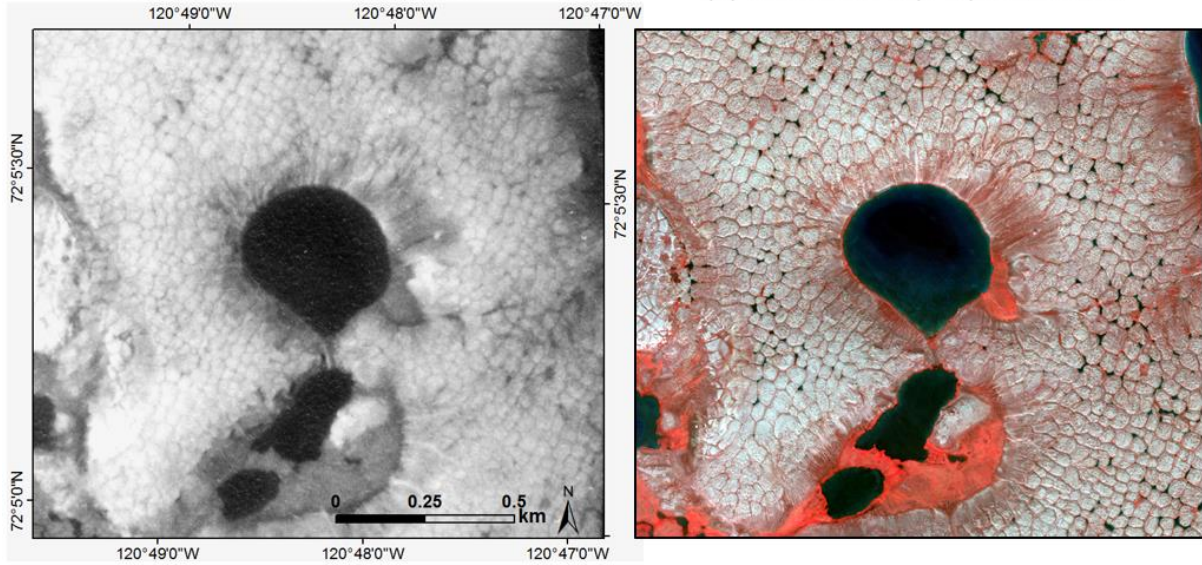
Figure S6. Comparison of historical air photos (a); recent 0.5 m resolution WorldView-1 panchromatic satellite imagery (b); Landsat SWIR and SWIR trend imagery (significant negative trends are shown in dark blue) (c-e); Sentinel-2 10 m satellite imagery (RGB = NIR, Red, Green) (f); and ArcticDEM elevations (g) for portions of high resolution study areas 1 and 3-8. Areas with continuous graminoid vegetation appear dark grey in the air photos (red in the Sentinel-2 image), while thermokarst lakes and ponds present a darker tone. WorldView-1 panchromatic imagery integrates both visible and near-infrared wavelengths, which causes this graminoid vegetation to appear brighter than in the air photos.



Area 3

(a) Air Photo 100k Aug 6, 1960

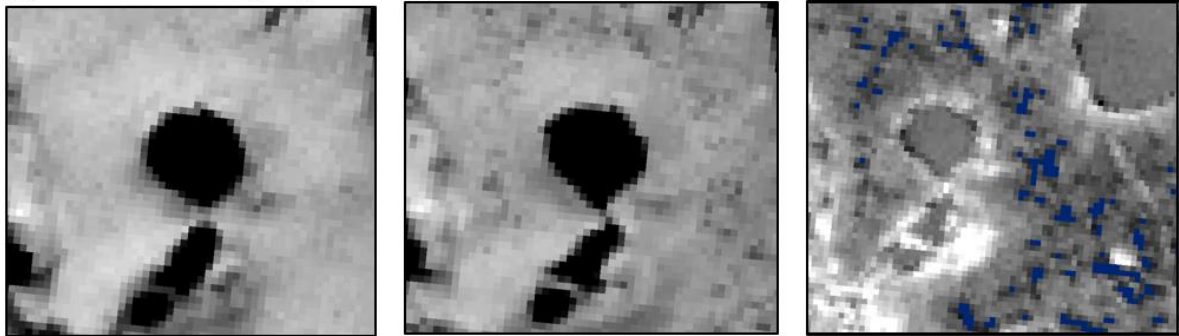
(b) WorldView-2 (2 m) Jul 31, 2017



(c) Landsat SWIR Aug 16, 1986

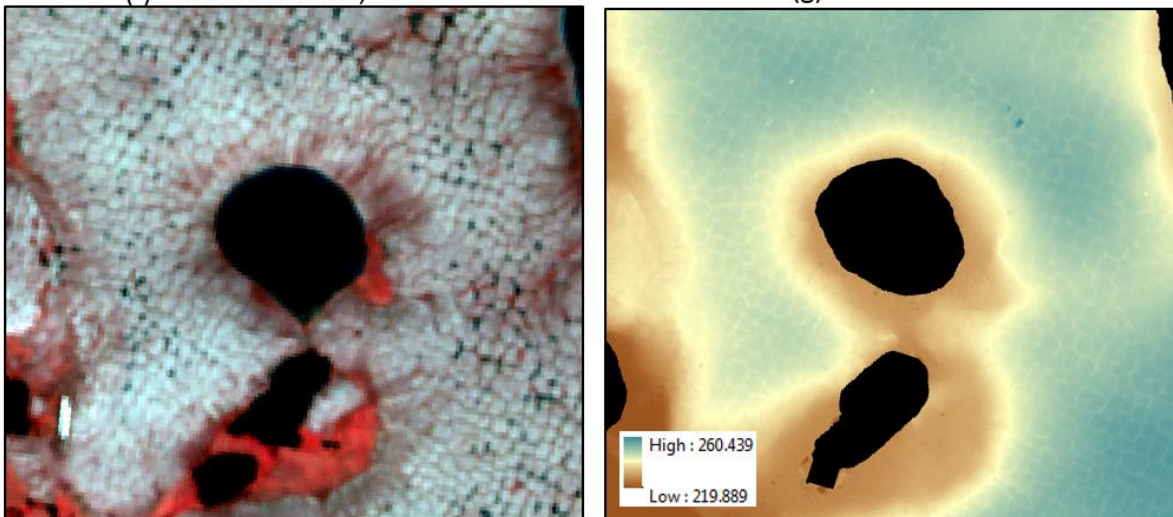
(d) Landsat SWIR Aug 10, 2013

(e) ~ 30-year SWIR trend



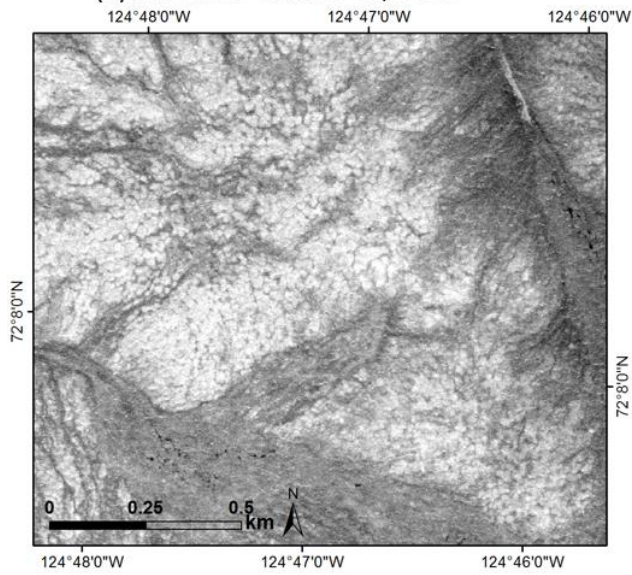
(f) Sentinel-2 Jul 19, 2017

(g) ArcticDEM

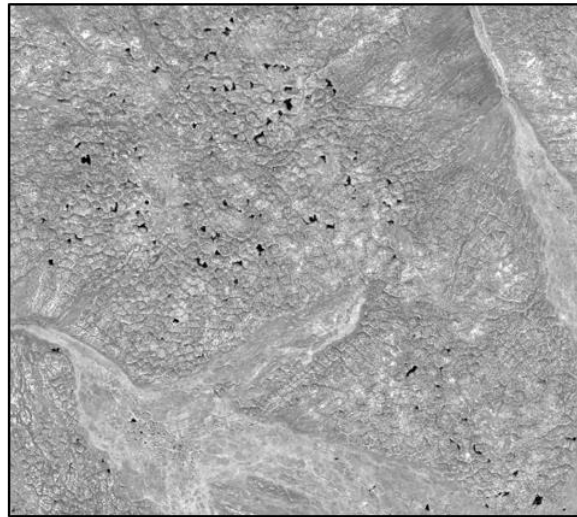


Area 4

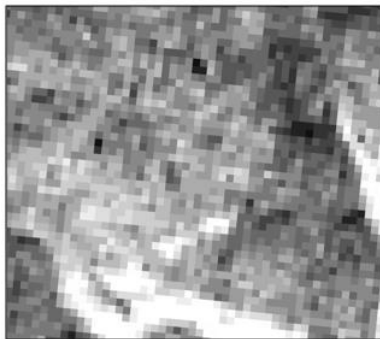
(a) Air Photo 60k Jul 14, 1958



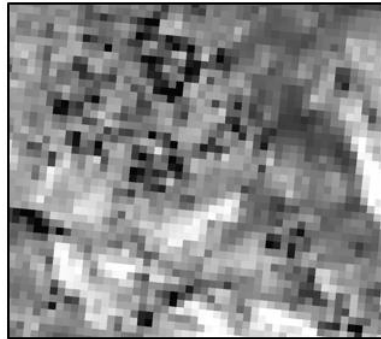
(b) WorldView-1 (0.5 m) Aug 10, 2013



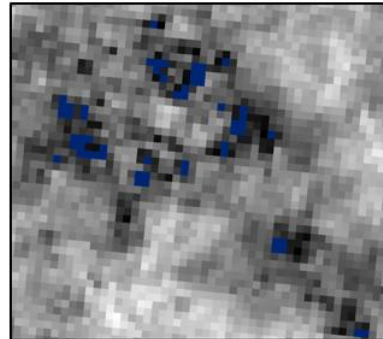
(c) Aug 5, 1986 Landsat SWIR



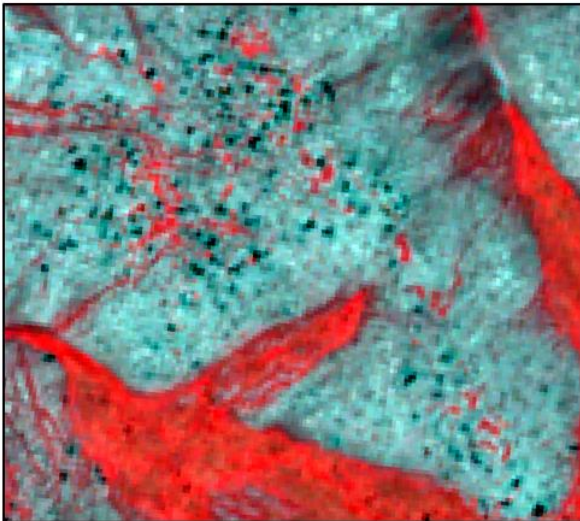
(d) Jul 15, 2015 Landsat SWIR



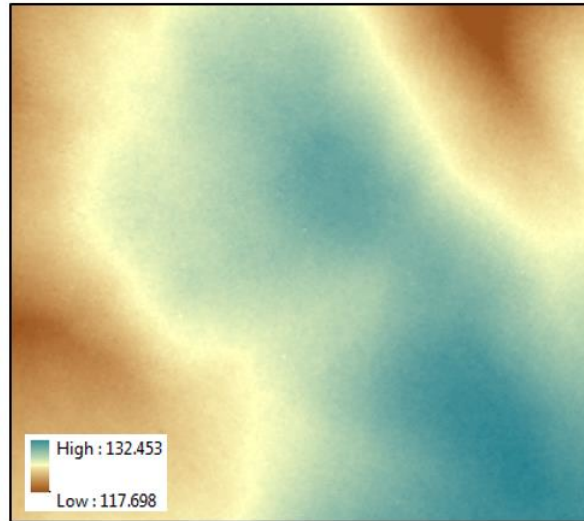
(e) ~ 30-year SWIR trend



(f) Sentinel-2 Jul 19, 2017

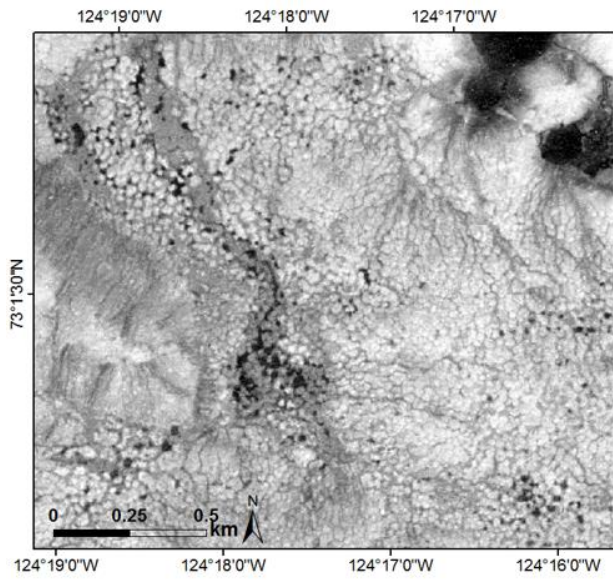


(g) ArcticDEM

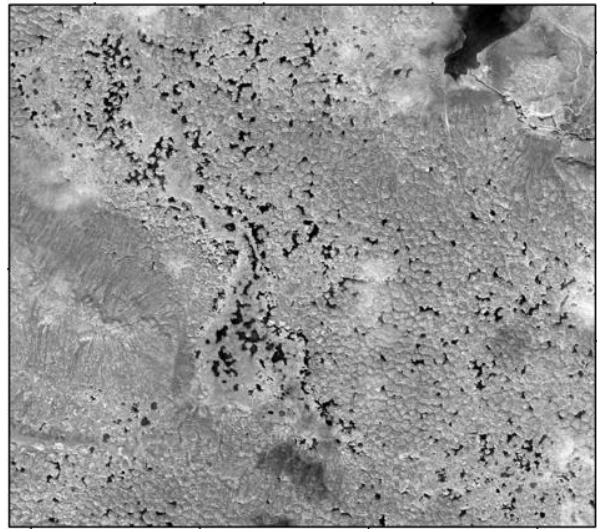


Area 5

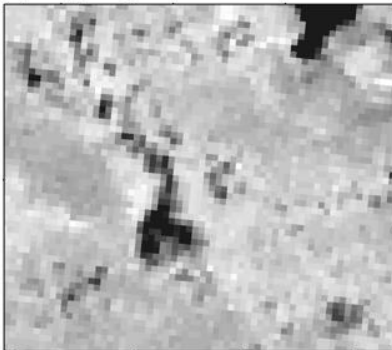
(a) Air Photo 100k Jul 29, 1961



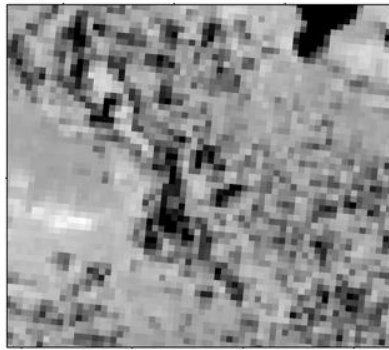
(b) WorldView-1 (0.5 m) Aug 19, 2014



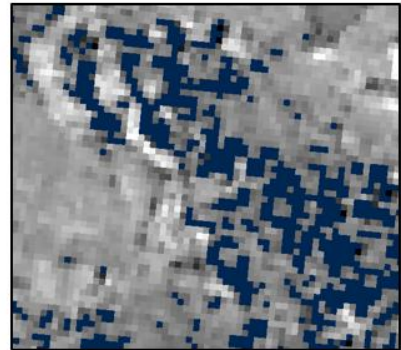
(c) Aug 17, 1986 Landsat SWIR



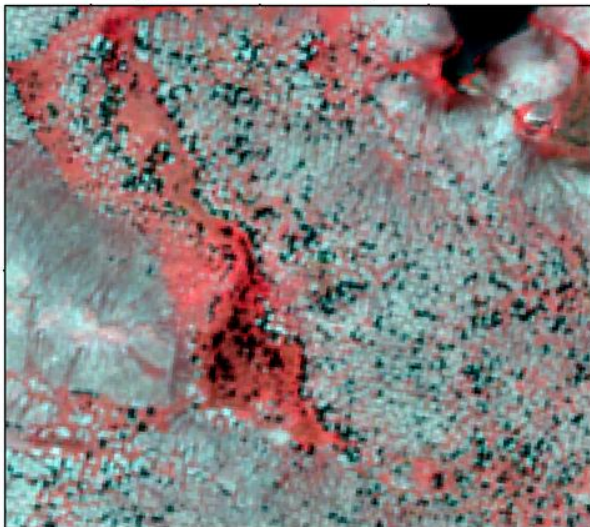
(d) Jul 27, 2016 Landsat SWIR



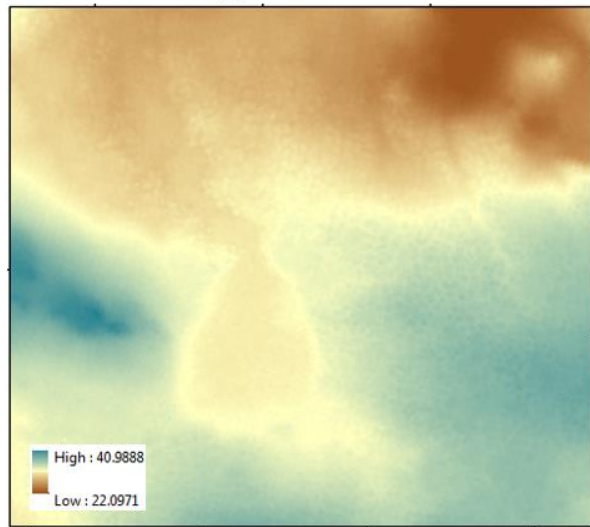
(e) ~ 30-year SWIR trend



(f) Sentinel-2 Jul 19, 2017



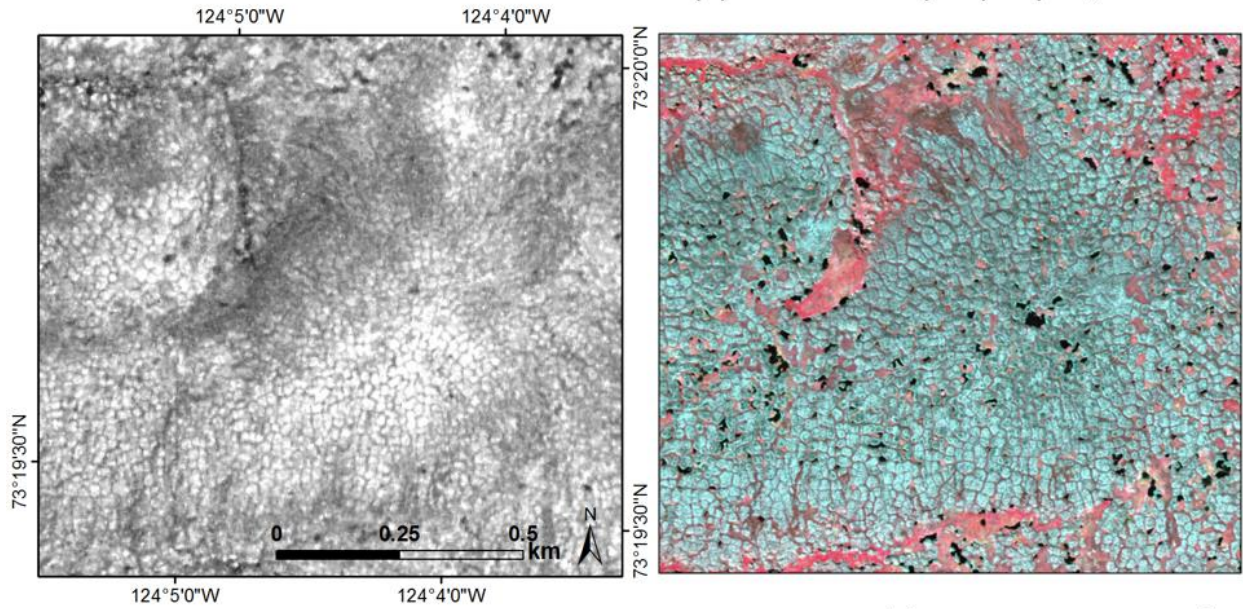
(g) ArcticDEM



Area 6

(a) Air Photo 100k Jul 29, 1961

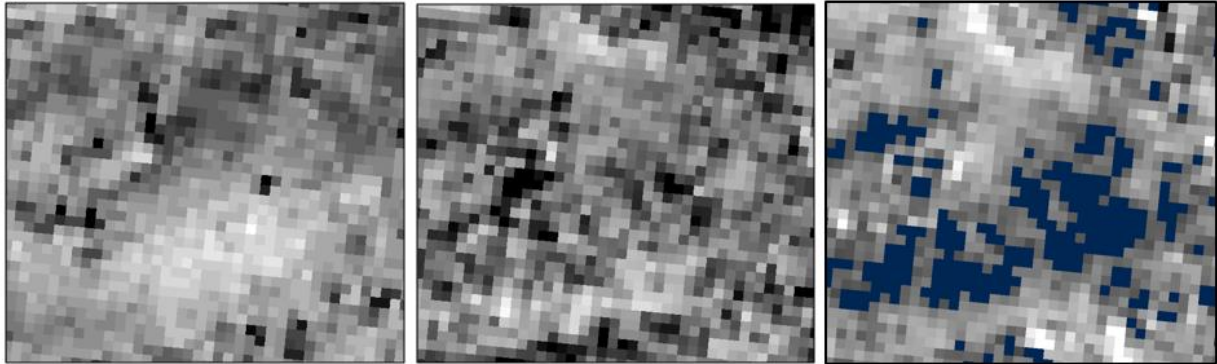
(b) WorldView-2 (2 m) July 30, 2012



(c) Aug 17, 1986 Landsat SWIR

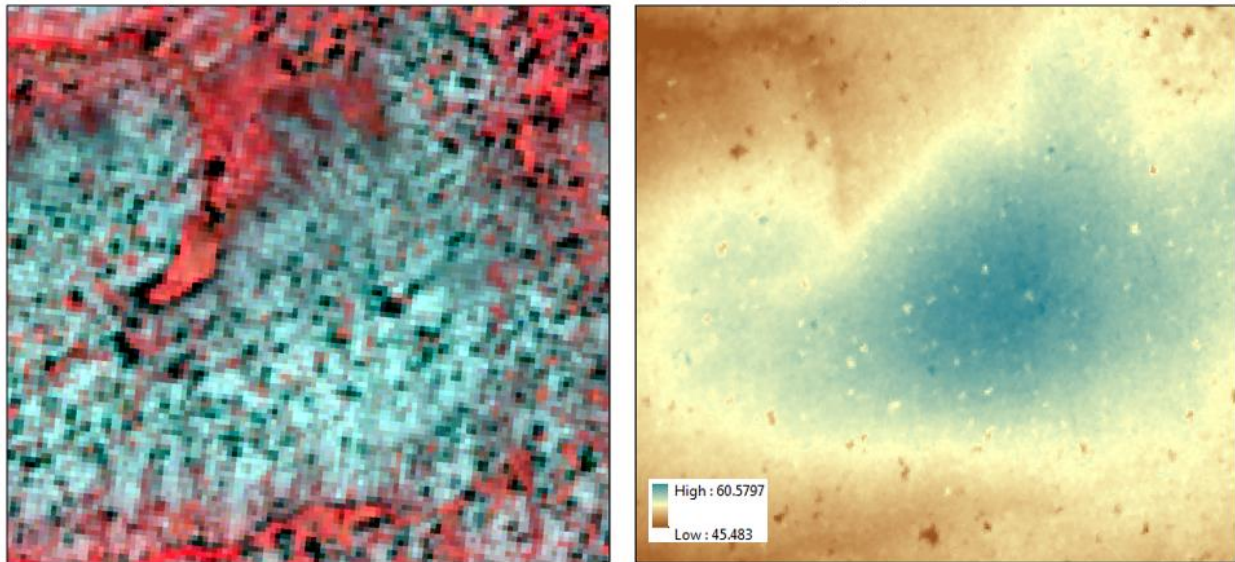
(d) Jul 27, 2016 Landsat SWIR

(e) ~ 30-year SWIR trend



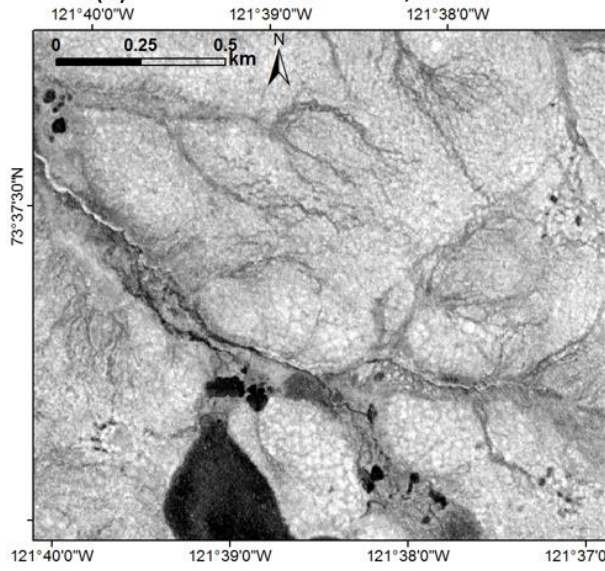
(f) Sentinel-2 Jul 19, 2017

(g) ArcticDEM

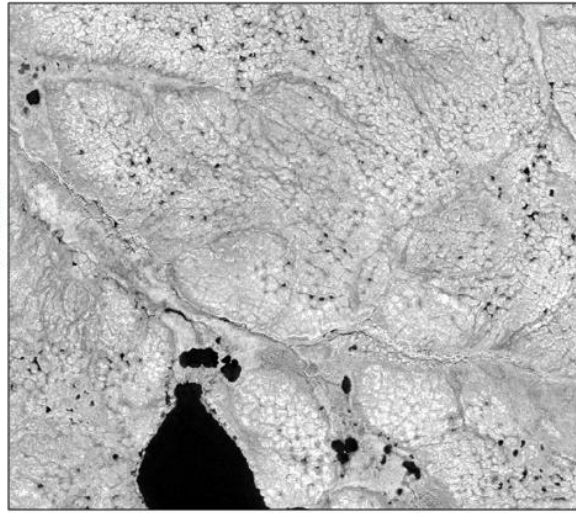


Area 7

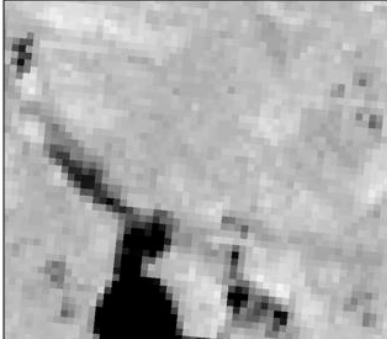
(a) Air Photo 100k Jul 29, 1961



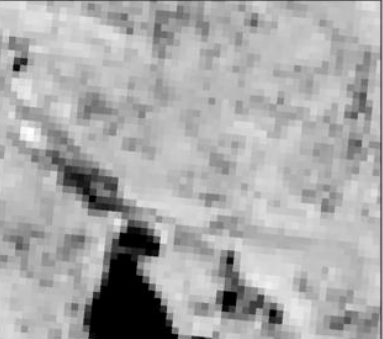
(b) WorldView-1 (0.5 m) Aug 20, 2014



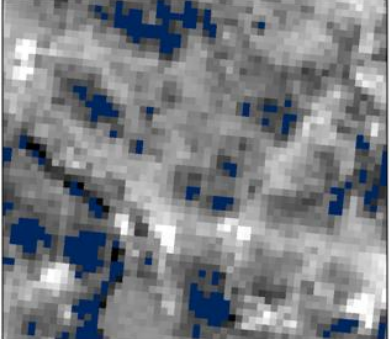
(c) Aug 14, 1986 Landsat SWIR



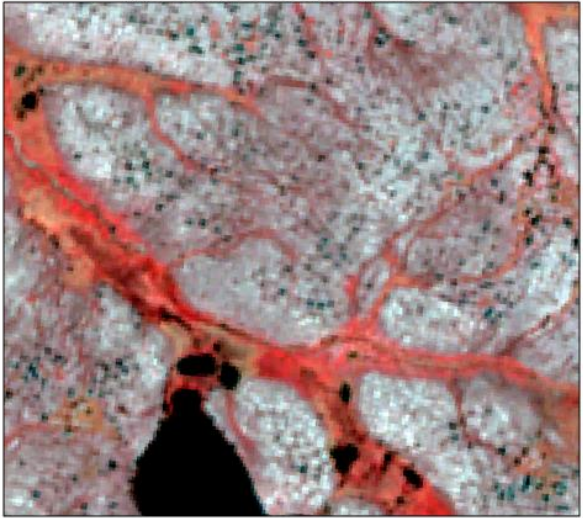
(d) Jul 27, 2016 Landsat SWIR



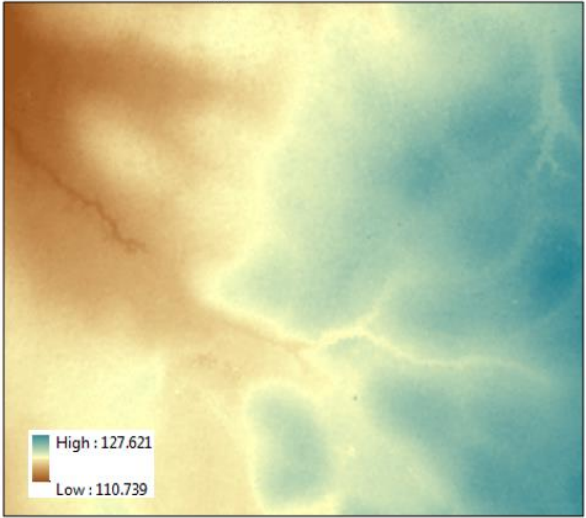
(e) ~ 30-year SWIR trend



(f) Sentinel-2 Jul 19, 2017

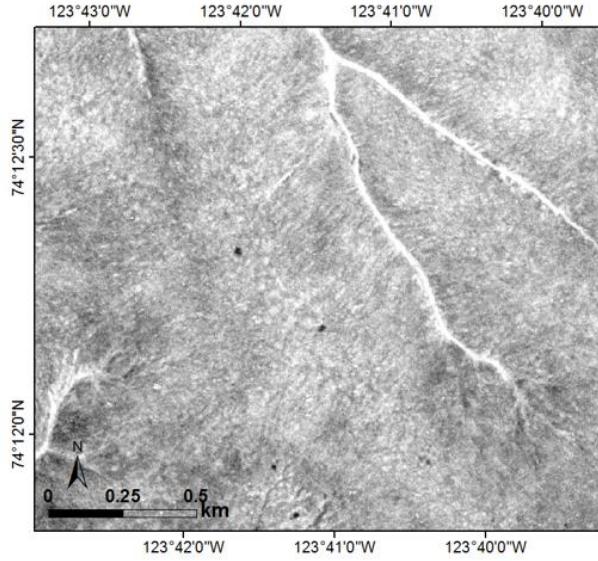


(g) ArcticDEM

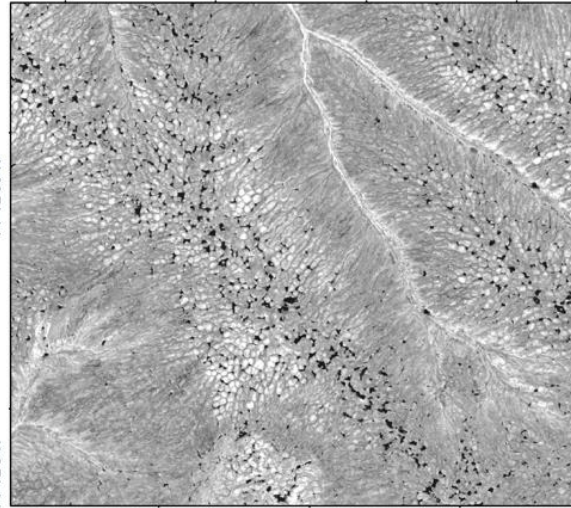


Area 8

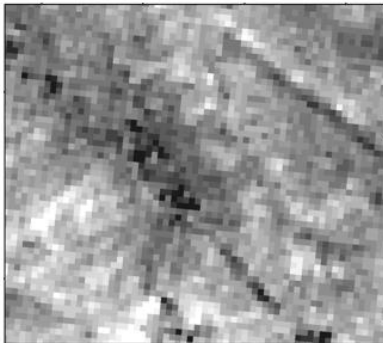
(a) Air Photo 100k Jul 29, 1961



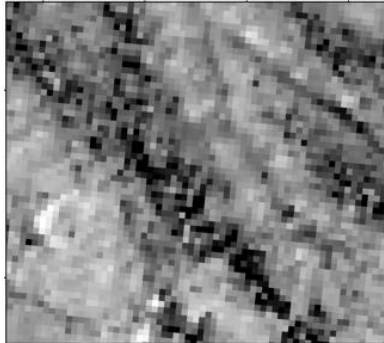
(b) WorldView-2 (0.5 m) Jul 22, 2015



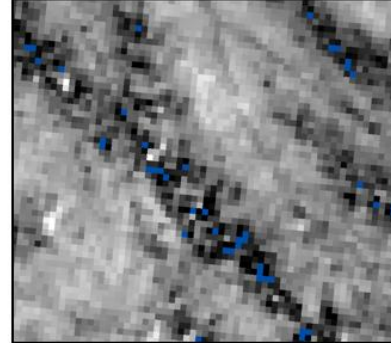
(c) Jul 18, 1986 Landsat SWIR



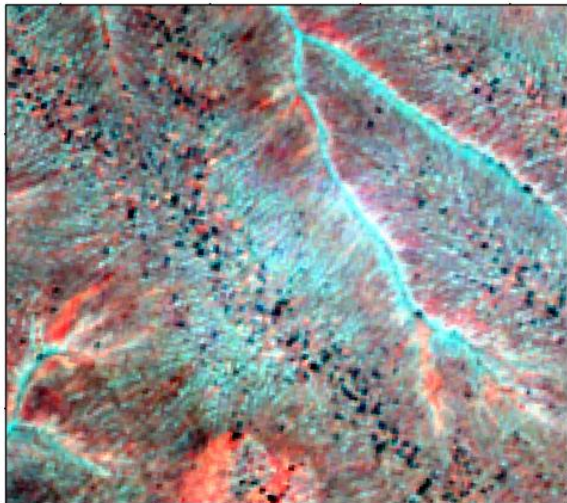
(d) Jul 27, 2016 Landsat SWIR



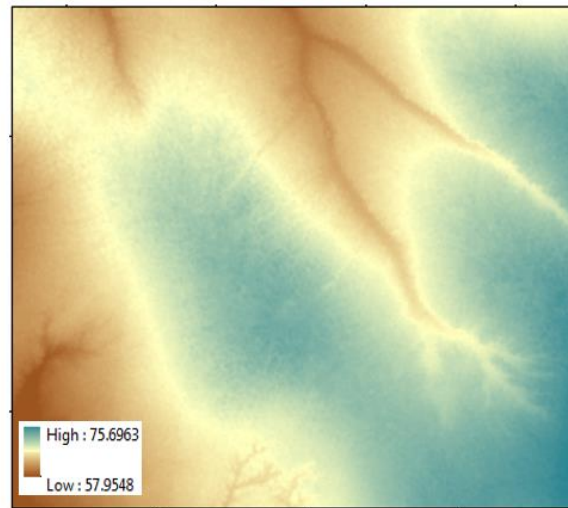
(e) ~ 30-year SWIR trend



(f) Sentinel-2 Jul 19, 2017



(g) ArcticDEM



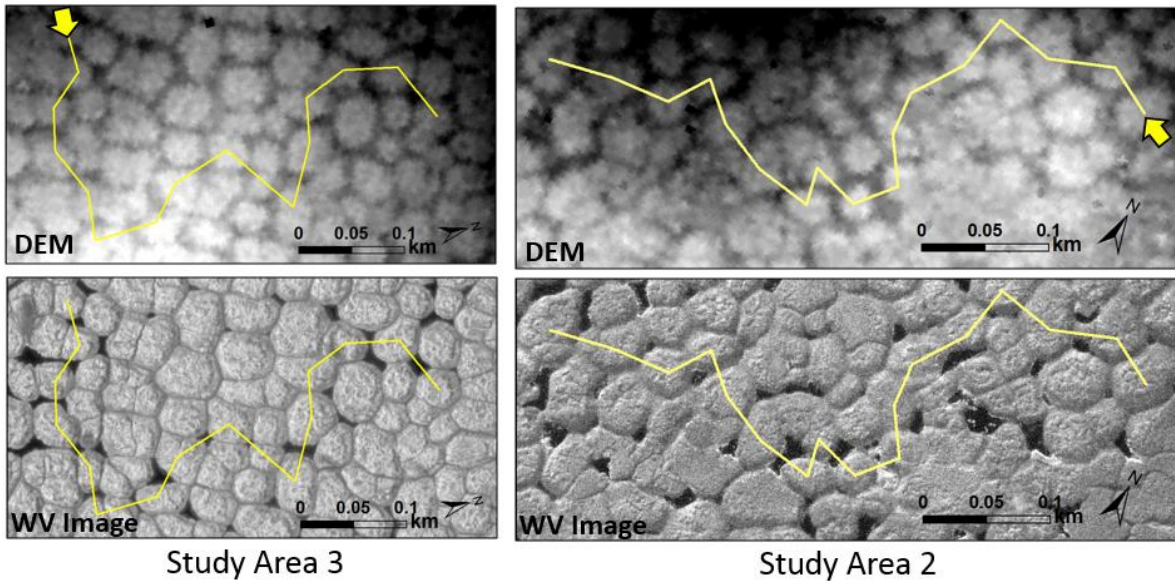
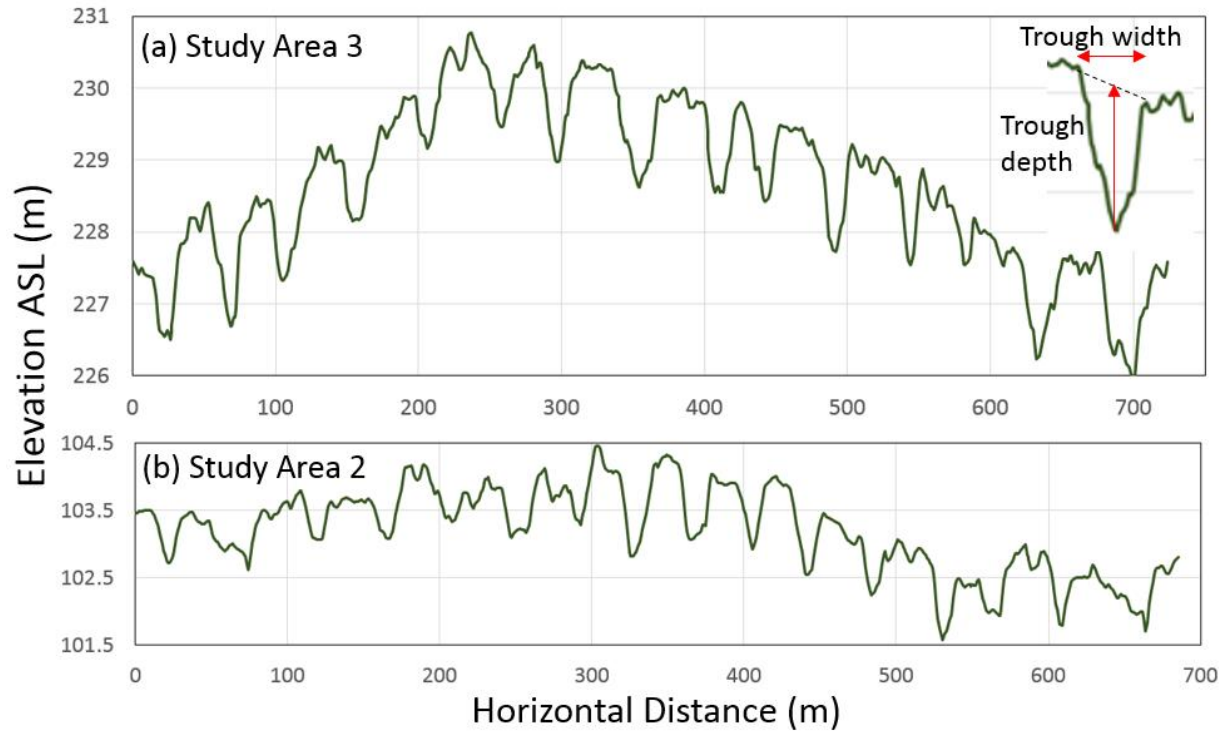


Figure S7. Two elevation profiles across degraded ice-wedge polygons extracted from the 2 m ArcticDEM product within relatively flat, upland terrain in study areas 2 and 3. Note the exaggerated vertical scale and that measured landscape slopes are generally less than 1%. Trough depth was measured vertically from the bottom of troughs to a line connecting the tops of adjacent polygons. Trough width represents the horizontal distance of this line. Corresponding ArcticDEM and 0.5 m WorldView imagery are shown at the bottom with transect lines and directions overlaid in yellow. Features submerged by shallow melt ponds are visible in the WorldView imagery, suggesting that the stereo-photogrammetric ArcticDEM should in most cases represent surface elevations below the melt ponds.

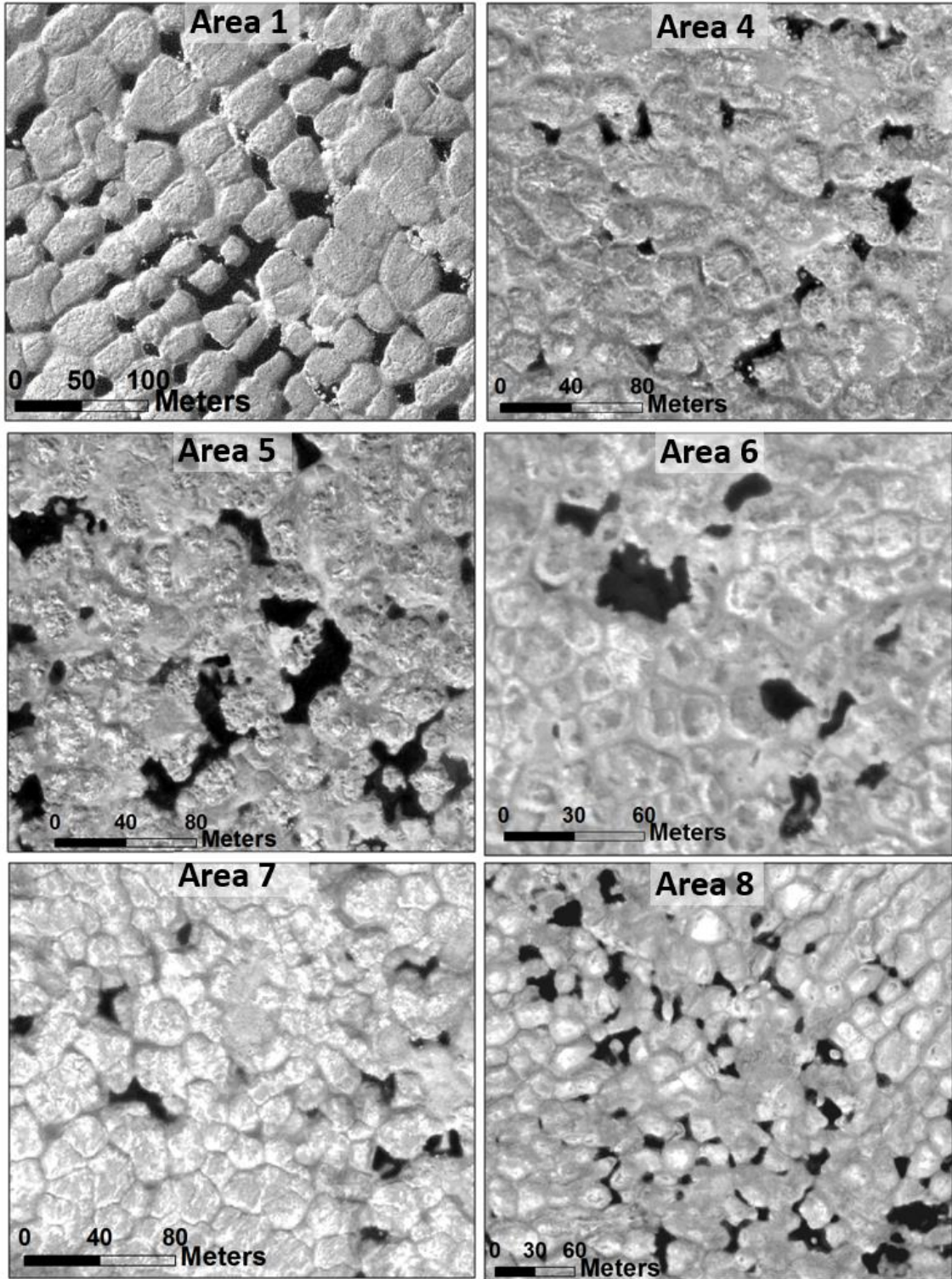


Figure S8. Recent (2012-2017) WorldView 0.5 m resolution satellite images within six of the study areas showing larger upland ice-wedge melt ponds where there was limited or no ponding observed in the 1958-1961 air photos.



Figure S9. Photo from August 2017 showing ice-wedge trough settlement in Aulavik National Park, north-central Banks Island (73.95°N , 119.85°W), a region in which little ice-wedge ponding was mapped using the Landsat trend method. Long fissures occur along the tops of ice wedge troughs due to ground subsidence and sloughing, as has also recently been observed on Ellesmere Island in the Canadian high-Arctic [51]. The photo was extracted from a 4K UAV video provided courtesy of Aurora Research Institute and Parks Canada Agency.

Table S1. Specifications for high resolution imagery and air photos covering the high resolution study areas. Study areas were delineated to exploit portions of the air photos providing the best contrast for identifying small ponds. As in the Landsat image collection, summer dates were selected to avoid the period of snowmelt and high spring runoff.

Study Site ID	Area (km ²)	Satellite	Resolution (m)	Date	Historical Air Photo Date
1	8.1	WorldView-1	0.5 (Pan)	August 11, 2013	July 25, 1961
2	12.4	WorldView-1	0.5 (Pan)	August 11, 2013	July 25, 1961
3	4.2	WorldView-2	0.5 (Pan) 2.0 (MS)	July 31, 2017	August 6, 1960
4	12.0	WorldView-1	0.5 (Pan)	August 10, 2013	July 14, 1958
5	5.3	WorldView-1	0.5 (Pan)	August 19, 2014	July 29, 1961
6	11.0	WorldView-2	0.5 (Pan) 2.0 (MS)	July 30, 2012	July 29, 1961
7	7.6	WorldView-1	0.5 (Pan)	August 20, 2014	July 29, 1961
8	10.4	WorldView-2	0.5 (Pan) 2.0 (MS)	July 22, 2015	July 29, 1961

Table S2. Thickness of material over massive ground ice, Banks Island where ice-wedge sites are shown in bold.

Site	Coordinates	Site type	Overburden thickness (cm) Mean (stdev)
1	10W0468993	Stony sandy silt till	74.07 (9.58)
1_IW	7978949	Ice-cored permafrost	63.25 (6.24)
2	10W0465719 7953493	Stony sandy silt till Ice-cored permafrost	127.27 (7.20)
3	10W0417040	Organic soil over silt	55.93 (15.89)
3_IW	7988551	Ice-rich permafrost	51.00 (6.48)
4	10W0457944 7960602	Gravelly till Ice-cored permafrost	180.13 (29.00)
5	10W0458013 7960362	Gravelly till Ice-cored permafrost	285.83 (188.13)

Table S3. Comparison of ice-wedge melt pond characteristics for eight upland study areas and two mapping periods on Bank Island. Averages represent values averaged among study areas.

Study Area ID	Area (km ²)	1958-1961 Air Photos			2013-2017 WorldView Satellite Imagery				Percent Change	
		Average pond area (m ²)	Pond area (ha) per km ² (or %)	Density (ponds/k m ²)	Average pond area (m ²)	Pond area (ha) per km ² (or %)	Density (ponds/km ²)	Largest New Pond (m ²)	Total pond area	Pond density
1	8.1	109	0.08	7.7	127	1.71	135.2	1376	1956%	1666%
2	12.4	179	0.07	4.0	112	1.90	170.2	1076	2592%	4206%
3	4.2	244	0.40	16.2	108	1.18	109.5	602	198%	576%
4	12.0	69	0.00	0.4	75	0.24	32.4	415	8356%	7680%
5	5.3	109	0.41	37.5	193	3.16	163.6	2040	675%	336%
6	11.0	84	0.19	23.1	109	0.90	82.5	1286	365%	257%
7	7.6	125	0.22	17.5	126	0.90	71.2	488	309%	307%
8	10.4	146	0.02	1.1	88	1.63	184.4	1174	10409%	17336%
Average	8.9	133	0.2	13.4	117	1.5	118.6	1057	923%	784%